Modelling of hybrid laser–GMA welding: review and challenges

Z. H. Rao[1], S. M. Liao[1] and H. L. Tsai*[2]

Hybrid welding, which is the integration of laser beam welding (LBW) and gas metal arc welding (GMAW), may minimise the disadvantages while retaining the advantages for each of the two welding technologies and, hence, has recently received increasing interest in the welding industry. However, the hybrid welding involves very complex transport phenomena which are inherited from each of LBW and GMAW and their interactions. The development of hybrid welding has been based on the trial and error procedure and so far rather limited numerical modelling on hybrid welding is available. This paper presents an up to date literature review on modelling of the hybrid welding including LBW and GMAW. Issues and challenges for a comprehensive hybrid welding model are discussed. With the advances of numerical techniques and computers, a comprehensive hybrid welding model can be developed as a useful tool for determining key process parameters and helping the elimination/reduction of possible weld defects.

Keywords: Hybrid welding, Laser welding, GMAW, Modelling

Introduction

The hybrid laser–gas metal arc (GMA) welding is formed by combining laser beam welding (LBW) and gas metal arc welding (GMAW),[1,2] as sketched in Fig. 1, which has received increasing interest in both academia and industry in recent years. In general, LBW encounters the poor gap bridgability and the metallurgical defects such as porosity, cracking, humping and undercutting.[3,4] As compared with LBW, GMAW has a higher heat input and lower energy density, leading to thermal distortion and a wider but shallower weld bead at relatively lower welding speeds.[3] The hybrid welding can decrease the disadvantages of each individual process, producing deep welding penetration, high welding speed, less deformation and high ability to bridge relatively large gaps resulting in higher robustness for industrial applications.[5,6] Furthermore, due to the addition of GMAW, the use of the hybrid welding can possibly lower the investment and costs through the reduction in the laser power.

Many experiments of the hybrid laser–GMA welding have been carried out with an attempt to identify the weldability of various base materials,[7–11] and the effects of operating parameters on the weld quality.[11–20] The experimental studies provided the useful information for the understanding and improvement of the hybrid welding. It was concluded that laser power and arc current, laser to arc power ratio and laser–arc interval should be set carefully to achieve the stable keyhole formation,[14] the high melting energy[18] and the improved weld quality.[11,12] The phenomena of the synergistic interaction between the laser beam and the electric arc were also observed.[14–16] The laser beam stabilised the arc even at the high welding speed.[15] The laser induced metal vapour enhanced the current conduction and reduced the arc voltage as blending into the arc plasma, and hence affected the features of metal transfer mode in the arc process.[16] The electric arc during the hybrid welding was found to be rooted at the laser radiation point, which squeezed the arc into a narrow range and concentrated the energy.[15] The arc current and hence the mode of metal transfer had a great influence on the weld bead and the process stability.[14,16] However, details of the physics involved in the observed phenomena cannot be obtained by experiments alone due to the non-transparent metal, the tiny and unstable keyhole, the high temperature plasma and the strong coupling of welding parameters in a transient manner. It is also rather costly and time consuming to develop the hybrid welding by using the trial and error procedure.

With the advances of numerical techniques and high power computers, the numerical method offers a convenient way to better understand the underlying mechanisms and optimise the process parameters for the success of the hybrid welding. So far, many numerical studies have been carried out on LBW and GMAW from various aspects, but rather limited numerical model on the hybrid welding is available. Because the hybrid laser–GMA welding couples both the characteristics and the synergistic interaction of the two processes, this paper begins with the review on modelling of LBW and GMAW, and then presents the current issues and challenges in modelling of the hybrid welding. The

[1]School of Energy Science and Engineering, Central South University, Changsha 410083, China
[2]Department of Mechanical and Aerospace Engineering, Missouri University of Science and Technology, Rolla, MO 65409, USA

*Corresponding author, email tsai@mst.edu

Published by Maney on behalf of the Institute
Received 13 December 2010; accepted 3 February 2011
DOI 10.1179/1362171811Y.0000000022

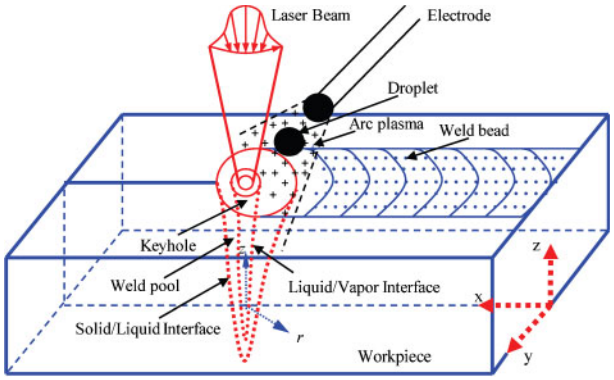

1 Schematic sketch of three-dimensional moving hybrid laser–GMA welding

physical process and fundamentals for each welding process are also discussed.

Modelling of LBW

During LBW, a high energy density laser beam impinges onto a workpiece and melts/vaporises it, and usually creates a 'keyhole' in the weld pool. A comprehensive LBW model should include the following chain of events: the moving laser irradiation; the intense melting/vaporisation of base metal; the laser induced plasma generation; keyhole formation and dynamics; the inverse bremsstrahlung (iB) absorption, Fresnel absorption and multiple reflections of the laser energy; melt flow and heat transfer in the weld pool; and fusion and solidification in the weldment. In addition, the keyhole surface and the top surface of the weld pool are highly deformable and change rapidly, resulting in the unstable surface phenomena. The above events coupled in a transient manner determine the highly complex nature of LBW modelling.

Numerous efforts have been attempted to simulate the different events during LBW, including the generation of plasma and plume,[21–27] the absorption of laser energy,[26,28–30] the keyhole generation, growth and collapse[28,31–40] and the weld pool dynamics.[41–45] In recent years, some integrated models[46–54] have been developed to predict the transport phenomena during LBW. Zhou *et al.*[46] developed a two-dimensional (2D) comprehensive LBW model, including Fresnel absorption and iB absorption of laser energy, melt flow and heat transfer, keyhole formation and collapse process, pressure balance, free surface, laser induced plasma vapour, thermal radiation and multiple reflections. In their model, the volume of fluid (VOF) technique[55] was employed to handle the transiently deformed weld pool surface, and the continuum formulation[56] was employed to handle fusion and solidification for the liquid region, mushy zone and solid region in the workpiece. The laser absorptions (i.e. iB absorption and Fresnel absorption) and the thermal radiation by the plasma in the keyhole were included by solving the plasma energy equation. The recoil pressure, Marangoni shear force, hydrodynamic force and hydrostatic force were considered as the driving forces for the melt flow in the weld pool. Some calculated results on the porosity formation[47,48] and the incorporation of the electromagnetic force to reduce porosity formation in LBW[49] were reported based on this model. Ki *et al.*[52] developed a three-dimensional (3D) LBW model to simulate the fluid flow and heat transfer. In their model, for the liquid/vapour interface the self-consistent evolution of the free surface boundary was predicted by using the level set approach, but the laser induced plasma was not considered. Based on the level set method and the assumption of the conical keyhole, Dasgupta and Mazumder[53] developed a multiple reflection model to simulate the CO_2 laser welding of zinc coated steel which took into account the plasma absorption of the laser energy by the iB mechanism. Amara and Fabbro[54] assumed the cross-section of the keyhole at each keyhole depth to be a circle with the depth dependent diameter and the centre position, and proposed a 3D model to simulate the liquid metal flow in LBW for an iron workpiece.

The predictive ability and accuracy of LBW models has greatly increased in recent years. It was claimed that the calculated results from the models were in agreement with the experimental results, including for the weld bead profiles and weld defects.[46–54] The successful modelling of LBW provides the vital basis for modelling the hybrid welding process. However, it is also found from the above review that the more accurate predictions for LBW are required. The full understanding on many phenomena in LBW has not yet been achieved, including, for example: the coupling of the moving laser beam, plasma and keyhole dynamics and the related fluid flow and energy transfer processes in the keyhole and the weld pool; the mechanisms leading to the formations of weld defects; and the selection of the optimal operating parameters.

Modelling of GMAW

In GMAW, a plasma arc is struck between the electrode and the workpiece through ionising the shielding gas by the imposed electric current. The electrode continuously fed downward is melted and forms a droplet at its tip that is periodically detached and transferred to the workpiece. A weld pool is gradually formed at the workpiece by the plasma arc and impinging droplets. Generally, modelling a GMAW process includes the following three events: the generation and evolution of arc plasma; the dynamic process of droplet formation, detachment, transfer and impingement onto the weld pool; and the dynamics of weld pool and the formation of weld bead. Apparently, the arc plasma interacts in a transient manner with the droplet and the weld pool during the GMAW process.

Numerous models have been developed to simulate the 2D stationary GMAW process[57–71] and 3D moving GMAW process.[72–77] Based on the VOF method[55] and the continuum formulation,[56] Zhu *et al.*[64] and Hu and Tsai[65,66] developed a comprehensive 2D GMAW model covering all the events, which is capable of simulating the interactive coupling between the arc plasma; the melting of the electrode; the droplet formation, detachment, transfer and impingement onto the workpiece; and the weld pool dynamics. The model was further extended to study the effects of welding current on the droplet generation and the metal transfer.[67,68] The calculated results showed that a higher current generated smaller droplets with higher detachment frequency. A stable one droplet per pulse metal transfer mode can be achieved by choosing a current with the proper waveform for the given welding condition. The model

predictions were quantitatively in consistent with the reported experimental results. Rao *et al.*[69–71] applied this model to predict GMAW with different shielding gases of argon and argon–helium mixtures. The effects of metal vapour were omitted for simplicity in order to obtain the intrinsic characteristics in the arc and the metal for various shielding gases. It was found that the increase in helium content in the mixture led to the formation of larger droplets and the decrease in droplet detachment frequency due to the arc contraction near the electrode, which was confirmed by the experimentally observed phenomena. The presence of metal vapour may change the thermophysical properties of the arc plasma[78–80] and, hence, the behaviours of the GMAW process.[81,82] Haidar[81] and Schnick *et al.*[82] focused on the effects of metal vapour in the argon arc, and found that the metal vapour decreased the arc temperature near the axis, which led to the decreases in heat flux density and current density at the workpiece.

For 3D moving GMAW, a simultaneous process involving the melting of the new solid base metal ahead of the molten pool and the solidification behind the weld pool leads to more complicated transport phenomena. There are a few articles[72–75] on modelling of 3D moving GMAW, but the impingement of the droplets into the weld pool was ignored or oversimplified. Hu *et al.*[76] and Rao *et al.*[77] developed 3D transient models to study the formation of ripples in the moving GMAW under different welding conditions, and the mechanism and the governing parameters of ripple formation were identified. In their models, the droplet was assumed as the sphere with the fixed size and impinging frequency. The transient arc plasma and droplet formation were not included in their models due to the excess computational time; instead, the results directly from experimental data were used in their studies. Therefore, although the prediction results from the models are reasonable, a more accurate and time efficient 3D model including all the events is required for simulating the moving GMAW process, which will further help improve the modelling of the hybrid laser–GMA welding process.

Modelling of hybrid laser–GMA welding

During the hybrid laser–GMA welding process, the laser irradiation is partially absorbed by the workpiece; a keyhole is generated in the workpiece; the plasma arc between the consumable electrode and the workpiece heats up and melts the base metal; and the droplets generated at the electrode tip are periodically detached and impinge onto the workpiece. A weld pool with keyhole is formed under the dynamical interaction of laser irradiation, plasma arc and filler droplets. An externally supplied shielding gas provides the protection of molten metal from exposing to the atmosphere. The successive weld pools create a weld bead and become a part of a welded joint when solidified at the workpiece surface. The numbers of parameters are greatly increased in the hybrid welding, mainly including laser beam parameters, electric power parameters, laser–arc interval, electrode diameter, wire feed speed, welding speed and shielding gas. Bagger and Olsen[6] reviewed the fundamental phenomena occurring in laser–arc hybrid welding and the principles for choosing the process parameters. Ribic *et al.*[83] reviewed the recent advances in hybrid welding with emphases on the physical interaction between laser and arc, and the effects of the combined laser–arc heat source on the welding process.

Fundamental understanding of the transport phenomena and the role of each parameter is critical for optimising the hybrid welding process. Numerical investigations were often carried out. Ribic *et al.*[84] developed a 3D heat transfer and fluid flow model for laser–GTA hybrid welding to understand the temperature field, cooling rates and mixing in the weld pool. Kong and Kovacevic[85] developed a 3D model to simulate the temperature field and thermally induced stress field in the workpiece during the hybrid laser–GTA process. By incorporating free surfaces based on the VOF method,[55] Gao *et al.*,[86] Cho and Na,[87] Cho *et al.*[88] and Cho and Farson[89] developed mathematical models to simulate the weld pool formation and flow patterns in hybrid laser–GMA welding. Generally, the typical phenomena of GMAW such as droplets impinging into the weld pool, electromagnetic force in the weld pool and the typical phenomena of LBW such as keyhole dynamics, iB absorption and Fresnel absorption were considered in these models. Surface tension, buoyancy, droplet impact force and recoil pressure were considered to calculate the melt flow patterns.

By using the VOF method, Zhou and Tsai[90] developed a 2D model for an axisymmetrical hybrid laser–GMA welding system. In their study, a hybrid welding of stainless steel was considered in which the laser power was 1·7 kW, the laser spot radius was 0·2 mm and the spherical droplets were assumed to be generated from the electrode at a certain diameter (0·35 mm) and impinging frequency (1000). Dynamics of weld pool fluid flow, energy transfer in keyhole plasma and interactions between the droplet impingement and weld pool were calculated as a function of time. It was found that the weld pool dynamics, cooling rate and final weld bead geometry were strongly affected by the droplet impingement in the hybrid welding. Figure 2 presents the comparison between the corresponding final solidified weld beads obtained by LBW alone and by the hybrid welding.[90] It is obvious that the hybrid welding effectively eliminates the formation of a pore near the root of the weld. The penetration depth in the hybrid welding is close to that in LBW, which indicates that the penetration depth is mainly affected by the characteristics of laser beam. The width of the weld bead (especially at the top) is much larger in the hybrid welding owing to the impingement of droplets and the electric arc heating. Zhou and Tsai also investigated the mixing and diffusion processes in the hybrid laser–GMA welding.[91] The effects of droplet parameters, such as droplet size, impinging frequency and impinging speed, on mixing/diffusion in the weld pool were studied.

Zhou *et al.*[92] further developed a 3D model for the hybrid laser–GMA welding. Figure 1 is a schematic sketch of the moving hybrid laser–GMA welding process. The laser with the power of 2·0 kW and the radius of 0·2 mm at the focus was employed, and the focus plane was at the top surface of the stainless steel workpiece. The electric arc with a power of 1 kW was behind the laser beam, and the distance between the laser beam centre and the arc centre was 1 mm. It was assumed that spherical droplets were detached at a certain diameter (0·25 mm) and frequency (172). In

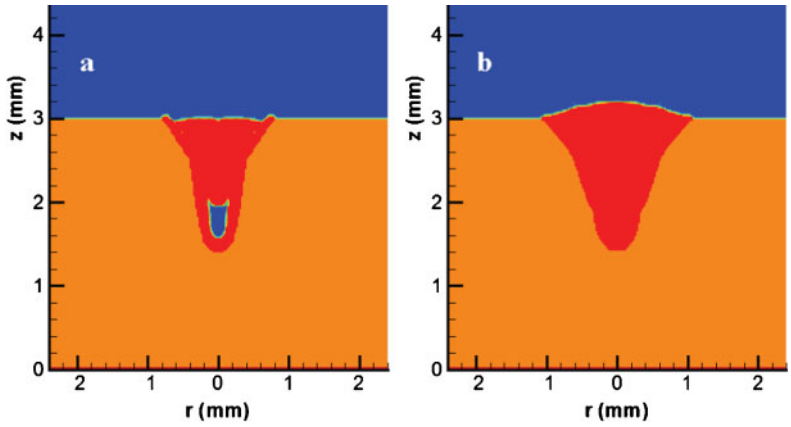

2 Comparison of weld bead shapes of *a* laser welding alone and *b* hybrid laser–GMA welding[90]

order to avoid possible end effects, the laser beam started to move at $x=1{\cdot}5$ mm, and the welding speed was $2{\cdot}5$ cm s^{-1}. The sequences of the temperature and velocity distributions in the x–z plane ($y=0$) are shown in Figs. 3 and 4 respectively.[92] As shown, a keyhole is created in front of the weld pool under the laser irradiation. As the droplet impinges into the weld pool, the thermal energy and momentum carried by the droplet merge into the weld pool, which in turn increase the temperatures near the impinging area and hence the weld pool size. Since the additional heat is obtained from the GMAW process, the solidification process of the weld pool is delayed which helps reduce the risk of the weld defects commonly observed in LBW, such as porosity and hot cracking.

In general, the above models can provide the reasonable predictions based on the comparison of weld shapes between the model calculation and the experimental observation. However, it should be pointed out that the existing models are far from the full solutions to the hybrid process. Developing a united model for the hybrid laser–GMA welding is very challenging, which cannot be formulated by only combining LBW model and GMAW model. In addition to the aforementioned events occurring in LBW alone and GMAW alone, the new events occurring in the hybrid process, such as the

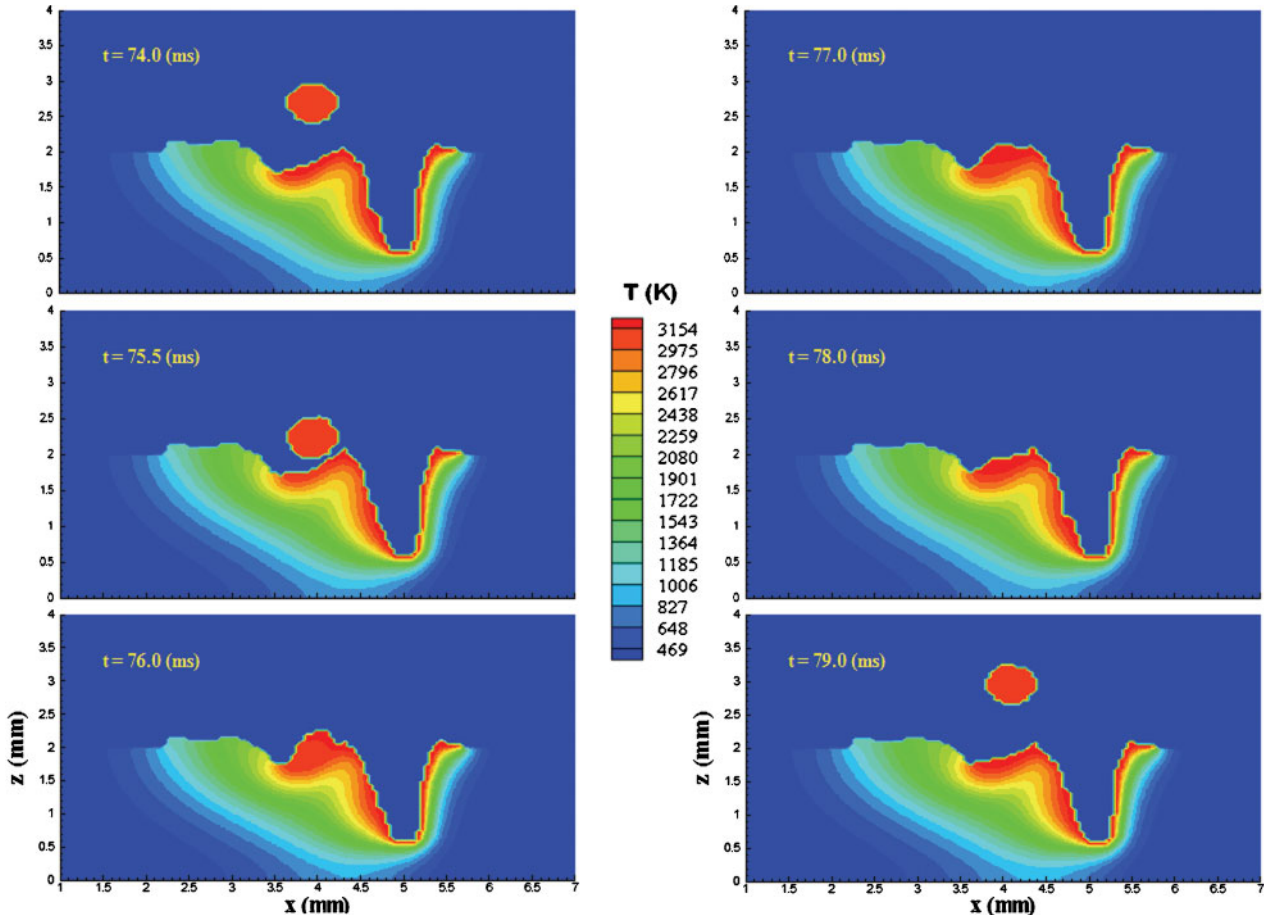

3 Sequence of temperature distribution showing impinging process of filler metal into weld pool in hybrid laser–GMA welding[92]

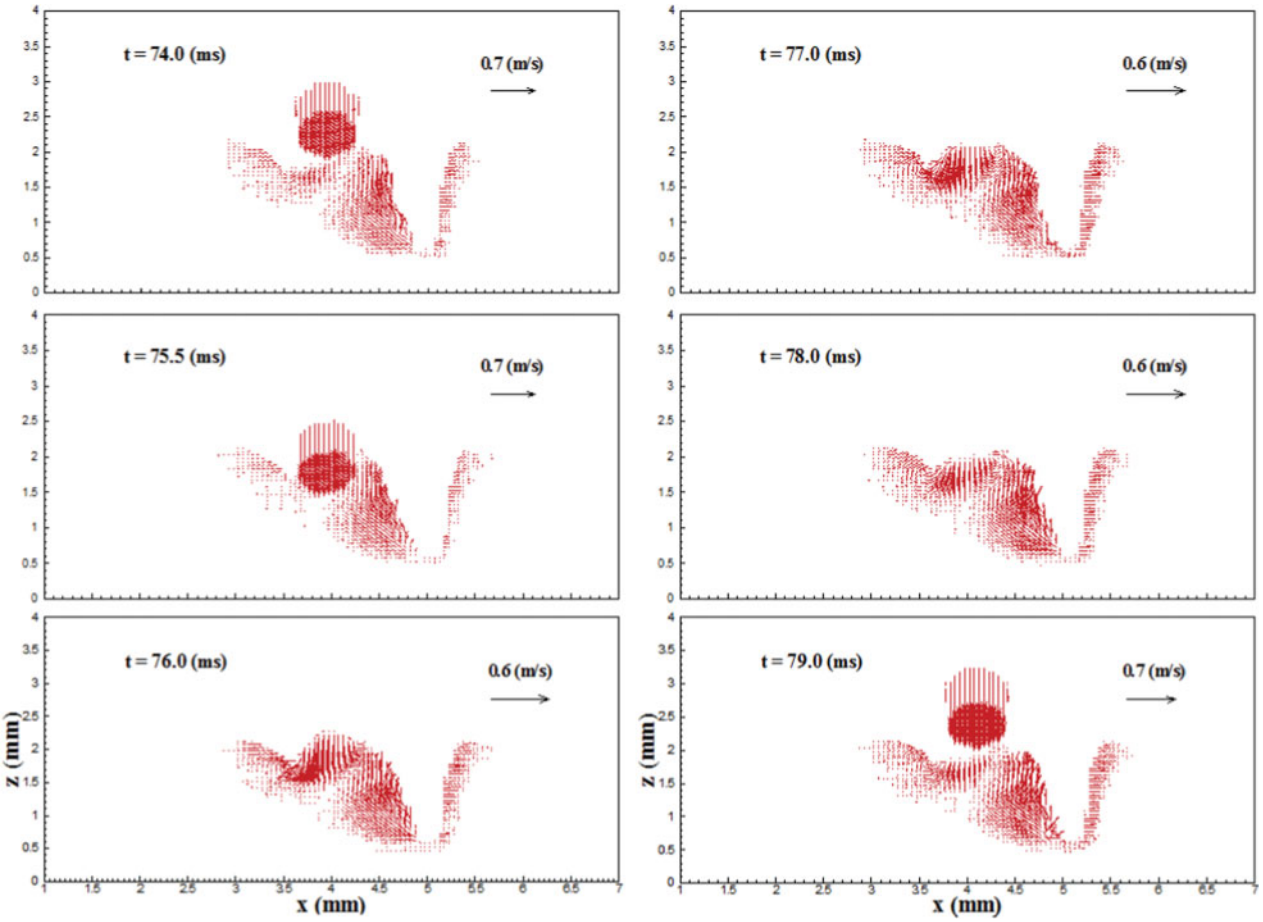

4 Corresponding velocity distribution for case as shown in Fig. 3[92]

synergistic interaction of the laser and the electric arc, and the effects of the coupled parameters, should be integrated into the model. Furthermore, the origins of some new events are not well understood and many important questions related to such modelling are still unanswered, which bring more difficulties for modelling of the hybrid laser–GMA welding. The main challenges for such modelling are as follows.

First, the synergistic interaction of the laser and the electric arc is not well understood in terms of the following phenomena: the electric arc preheats the base metal that enhances the absorption of the laser energy by the target metal; the electric arc dilutes the laser induced plasma and hence reduces the ability of the plasma to absorb and reflect the laser energy; the laser beam stabilises the electric arc; the laser induced metal vapour and plasma distort the electric arc structure; and the synergistic interaction of laser–arc changes the energy transfer and hence the welding process.

Second, the laser beam and the laser induced metal vapour significantly influence the features of metal transfer, but the underlying physics is still unclear. The transient arc plasma and droplet generation were ignored, and/or the droplets were assumed to impinge into the weld pool at a fixed size and frequency in the existing models, which fail to couple the generation of arc plasma, droplet formation, detachment and transfer during the hybrid welding.

Third, the effects of shielding gas, including its composition, flow rate and injecting direction, are still unclear. The shielding gas has significant influences on the plasma formation, the arc stability and hence the weld quality in the hybrid welding, which depend on the intrinsic properties of shielding gas. However, the effects of shielding gas in the hybrid welding are contradictory in some functions for the individual welding process, which requires further research to reduce the plasma shielding effect for the laser and also enhance the electric arc stability.

Finally, a real united model of hybrid laser–GMA welding will need an excess computation time. Therefore, more advanced computer technology and a more time efficient computation method are required.

Summary

In summary, the advantages of hybrid laser–GMA welding over LBW alone include higher process stability, higher bridgeability, less porosity and cracking and greater flexibility. The advantages of the hybrid welding over GMAW include higher welding speeds, deeper penetration, lower thermal input, higher tensile strength and narrower weld seams. To optimise the welding process and obtain the high quality weldments, a fundamental understanding to the complex phenomena in the hybrid welding process is essential. Since the trial and error method is time consuming and costly, the numerical technique is an important method that can provide detailed information for improving the process.

So far, limited efforts have been performed to simulate and understand the hybrid laser–GMA welding process. The existing models are far from the full solutions to the hybrid process, and many important questions related to modelling of the hybrid welding are still unanswered, including the synergistic interaction

of laser–arc, the features of metal transfer, the behaviours of shielding gas and the advanced numerical methods. Hence, there are many challenges for modelling of hybrid laser–GMA welding. Apparently, further work is required to understand and tackle the hybrid welding process more efficiently in the future. By combining numerical simulations and experiments, the key operating parameters can be determined and optimised. This is of great significance for the innovation in the metal joining technique and the advancement in producing high quality weldments.

References

1. W. M. Steen: *J. Appl. Phys.*, 1980, **5**, 5636–5641.
2. J. Matsuda, M. Katsumura, M. Hamazaki and S. Nagata: *Join. Mater.*, 1988, **7**, 31–34.
3. R. L. O'Brien: in 'Welding handbook', 8th edn, Vol. 2, 'Welding process'; 1991, Miami, FL, American Welding Society.
4. H. Zhao, D. R. White and T. DebRoy: *Int. Mater. Rev.*, 1999, **44**, 238–266.
5. J. Tusek and M. Suban: *Sci. Technol. Weld. Join.*, 1999, **4**, 308–311.
6. C. Bagger and F. O. Olsen: *J. Laser Appl.*, 2005, **17**, 2–14.
7. M. Gao, X. Y. Zeng, B. Tan and J. C. Feng: *Sci. Technol. Weld. Join.*, 2009, **14**, 274–281.
8. U. Dilthey, F. Lueder and A. Wieschemann: *Aluminum*, 1999, **75**, 64–75.
9. B. Hu and I. M. Richardson: *Mater. Sci. Eng. A*, 2007, **A459**, 94–100.
10. C. Roepke and S. Liu: *Weld. J.*, 2009, **88**, 159s–167s.
11. P. L. Moore, D. S. Howse and E. R. Wallach: *Sci. Technol. Weld. Join.*, 2004, **9**, 314–322.
12. G. L. Qin, Z. Lei and S. Y. Lin: *Sci. Technol. Weld. Join.*, 2007, **12**, 79–86.
13. G. Tani, G. Campana, A. Fortunato and A. Ascari: *Appl. Surf. Sci.*, 2007, **253**, 8050–8053.
14. G. Campana, A. Fortunato, A. Ascari, G. Tani and L. Tomesani: *J. Mater. Process. Technol.*, 2007, **191**, 111–113.
15. M. Ono, Y. Shinbo, A. Yoshitake and M. Ohmura: *NKK Tech. Rev.*, 2002, **86**, 8–12.
16. M. El-Rayes, C. Walz and G. Sepold: *Weld. J.*, 2004, **83**, 147s–153s.
17. H. W. Choi, D. F. Farson and M. H. Cho: *Weld. J.*, 2006, **85**, 174s–179s.
18. M. Gao, X. Y. Zeng and Q. W. Hu: *Sci. Technol. Weld. Join.*, 2006, **11**, 517–522.
19. L. Zhao, T. Sugino, G. Arakane and S. Tsukamoto: *Sci. Technol. Weld. Join.*, 2009, **14**, 457–467.
20. C. Li, K. Muneharua, S. Takao and H. Kouji: *Mater. Des.*, 2009, **30**, 109–114.
21. A. Poueyo-Verwaerde, R. Fabbro and G. Deshors: *J. Appl. Phys.*, 1993, **74**, 5773–5780.
22. M. Beck, P. Berger and H. Hügel: *J. Phys. D: Appl. Phys.*, 1995, **28**, 2430–2442.
23. C. Tix and G. Simon: *Phys. Rev. E*, 1994, **50E**, 453–462.
24. J. Dowden, P. Kapadiat and N. Postacioglu: *J. Phys. D: Appl. Phys.*, 1989, **22**, 741–749.
25. C. Tix and G. Simon: *J. Phys. D: Appl. Phys.*, 1993, **26**, 2066–2074.
26. U. Dilthey, A. Goumeniouk, V. Lopota and G. Turichin: *J. Phys. D: Appl. Phys.*, 2000, **33**, 2747–2753.
27. K. R. Kim and D. F. Farson: *J. Appl. Phys.*, 2001, **89**, 681–688.
28. A. Kaplan: *J. Phys. D: App. Phys.*, 1994, **27**, 1805–1814.
29. P. Solana and G. Negro: *J. Phys. D: Appl. Phys.*, 1997, **30**, 3216–3222.
30. R. Fabbro and K. Chouf: *J. Appl. Phys.*, 2000, **87**, 4075–4083.
31. V. Semak and A. Matsunawa: *J. Phys. D: Appl. Phys.*, 1997, **30**, 2541–2552.
32. S. Basu and T. DebRoy: *J. Appl. Phys.*, 1992, **72**, 3317–3322.
33. X. Jin, L. Li and Y. Zhang: *Int. J. Heat Mass Transf.*, 2003, **46**, 15–22.
34. P. S. Wei, T. H. Wu and Y. T. Chow: *ASME J. Heat Transf.*, 1990, **112**, 163–168.
35. J. Dowden, W. S. Chang, P. Kapadia and C. Strange: *J. Phys. D: Appl. Phys.*, 1991, **24**, 519–532.
36. T. Klein, M. Vicanek and G. Simon: *J. Phys. D: Appl. Phys.*, 1996, **29**, 322–332.
37. K. N. Lankalapalli, J. F. Tu and M. Garther: *J. Phys. D: Appl. Phys.*, 1996, **29**, 1831–1841.
38. H. Zhao and T. DebRoy: *J. Appl. Phys.*, 2003, **93**, 10089–10096.
39. R. Rai, G. G. Roy and T. DebRoy: *J. Appl. Phys.*, 2007, **101**, 054909.
40. R. Rai, S. M. Kelly, R. P. Martukanitz and T. DebRoy: *Metall. Mater. Trans. A*, 2008, **39A**, 98–112.
41. N. Postacioglu, P. Kapadia, M. Davis and J. Dowden: *J. Phys. D: Appl. Phys.*, 1987, **20**, 340–345.
42. A. Kar and J. Mazumder: *J. Appl. Phys.*, 1995, **78**, 6353–6360.
43. W. Pecharapay and A. Kar: *J. Phys. D: Appl. Phys.*, 1997, **30**, 3322–3329.
44. J. Kroos, U. Gratzke and G. Simon: *J. Phys. D: Appl. Phys.*, 1993, **26**, 474–480.
45. H. Ki, P. S. Mohanty and J. Mazumder: *Metall. Mater. Trans. A*, 2002, **33A**, 1831–1842.
46. J. Zhou, H. L. Tsai and P. C. Wang: *ASME J. Heat Transf.*, 2006, **128**, 680–690.
47. J. Zhou and H. L. Tsai: *ASME J. Heat Transf.*, 2007, **129**, 1014–1024.
48. J. Zhou and H. L. Tsai: *J. Phys. D: Appl. Phys.*, 2006, **39**, 5338–5355.
49. J. Zhou and H. L. Tsai: *Int. J. Heat Mass Transf.*, 2007, **50**, 2217–2235.
50. E. H. Amara and A. Bendib: *J. Phys. D: Appl. Phys.*, 2002, **35**, 272–280.
51. X. Chen and H. X. Wang: *J. Phys. D: Appl. Phys.*, 2003, **36**, 1634–1643.
52. H. Ki, P. S. Mohanty and J. Mazumder: *Metall. Mater. Trans. A*, 2002, **33A**, 1817–1830.
53. A. K. Dasgupta and J. Mazumder: *J. Appl. Phys.*, 2007, **102**, 053108.
54. E. H. Amara and R. Fabbro: *J. Phys. D: Appl. Phys.*, 2008, **41**, 055503.
55. D. B. Kothe, R. C. Mjolsness and M. D. Torrey: Report LA-12007-MS, Los Alamos National Laboratory, Los Alamos, NM, USA, 1991.
56. K. C. Chiang and H. L. Tsai: *Int. J. Heat Mass Transf.*, 1992, **35**, 1763–1769.
57. M. C. Tsao and C. S. Wu: *Weld. J.*, 1988, **67**, 70s–75s.
58. J. Jaidi and P. Dutta: *Numer. Heat Transf. A*, 2001, **40**, 543–562.
59. Y. Wang, Q. Shi and H. L. Tsai: *Metall. Mater. Trans. B*, 2001, **32B**, 145–161.
60. Y. Wang and H. L. Tsai: *Int. J. Heat Mass Transf.*, 2001, **44**, 2067–2080.
61. Y. Wang and H. L. Tsai: *Metall. Mater. Trans. B*, 2001, **32B**, 501–515.
62. H. G. Fan and R. Kovacevic: *J. Phys. D: Appl. Phys.*, 2004, **37**, 2531–2544.
63. H. G. Fan and R. Kovacevic: *Metall. Mater. Trans. B*, 1999, **30B**, 791–801.
64. F. L. Zhu, H. L. Tsai, S. P. Marin and P. C. Wang: *Prog. Comput. Fluid Dyn.*, 2004, **4**, 99–117.
65. J. Hu and H. L. Tsai: *Int. J. Heat Mass Transf.*, 2007, **50**, 833–846.
66. J. Hu and H. L. Tsai: *Int. J. Heat Mass Transf.*, 2007, **50**, 808–820.
67. J. Hu and H. L. Tsai: *J. Appl. Phys.*, 2006, **100**, 053304.
68. J. Hu and H. L. Tsai: *ASME J. Heat Transf.*, 2007, **129**, 1025–1035.
69. Z. H. Rao, J. Hu, S. M. Liao and H. L. Tsai: *Int. J. Heat Mass Transf.*, 2010, **53**, 5707–5721.
70. Z. H. Rao, J. Hu, S. M. Liao and H. L. Tsai: *Int. J. Heat Mass Transf.*, 2010, **53**, 5722–5732.
71. Z. H. Rao, S. M. Liao and H. L. Tsai: *J. Appl. Phys.*, 2010, **107**, 044902.
72. J. W. Kim and S. J. Na: *ASME J. Eng. Ind.*, 1994, **116**, 78–85.
73. M. Ushio and C. S. Wu: *Metall. Mater. Trans. B*, 1997, **28B**, 509–519.
74. S. Ohring and H. J. Lugt: *Weld. J.*, 2000, **79**, 416s–424s.
75. Z. Cao, Z. Yang and X. L. Chen: *Weld. J.*, 2004, **83**, 169s–176s.
76. J. Hu, H. Guo and H. L. Tsai: *Int. J. Heat Mass Transf.*, 2008, **51**, 2537–2552.
77. Z. H. Rao, J. Zhou, S. M. Liao and H. L. Tsai: *J. Appl. Phys.*, 2010, **107**, 054905.
78. G. J. Dunn and T. W. Eagar: *Metall. Mater. Trans. A*, 1986, **17A**, 1865–1871.
79. A. B. Murphy, M. Tanaka, K. Yamamoto, S. Tashiro, T. Sato and J. J. Lowke: *J. Phys. D: Appl. Phys.*, 2009, **42**, 194006.
80. K. Yamamoto, M. Tanaka, S. Tashiro, K. Nakata, K. Yamazaki, E. Yamamoto, K. Suzuki and A. B. Murphy: *Sci. Technol. Weld. Join.*, 2008, **13**, 566–572.
81. J. Haidar: *J. Phys. D: Appl. Phys.*, 2010, **43**, 165204.
82. M. Schnick, U. Füssel, M. Hertel, A. Spille-Kohoff and A. B. Murphy: *J. Phys. D: Appl. Phys.*, 2010, **43**, 022001.
83. B. Ribic, T. A. Palmer and T. DebRoy: *Int. Mater. Rev.*, 2009, **54**, 223–244.
84. B. Ribic, R. Rai and T. DebRoy: *Sci. Technol. Weld. Join.*, 2008, **13**, 683–693.
85. F. Kong and R. Kovacevic: *J. Mater. Process. Technol.*, 2010, **210**, 941–950.
86. Z. Gao, Y. Wu and J. Huang: *Int. J. Adv. Manuf. Technol.*, 2009, **44**, 870–879.
87. J. H. Cho and S. J. Na: *Weld. J.*, 2009, **88**, 35s–43s.
88. W. Cho, S. Na, M. Cho and J. Lee: *Comput. Mater. Sci.*, 2010, **49**, 792–800.
89. M. H. Cho and D. F. Farson: *Weld. J.*, 2007, **86**, 253s–262s.
90. J. Zhou and H. L. Tsai: *Int. J. Heat Mass Transf.*, 2008, **51**, 4353–4366.
91. J. Zhou and H. L. Tsai: *J. Phys. D: Appl. Phys.*, 2009, **42**, 095502.
92. J. Zhou, H. L. Tsai, P. C. Wang, R. J. Menassa and S. P. Marin: ICALEO 2003, Jacksonville, FL, USA, October 2003, Sec. A, 135–141.